HHS Public Access

Author manuscript

Nat Neurosci. Author manuscript; available in PMC 2010 October 01.

Published in final edited form as:

Nat Neurosci. 2010 April ; 13(4): 439–449. doi:10.1038/nn.2489.

Diversity and Wiring Variability of Olfactory Local Interneurons in the *Drosophila* Antennal Lobe

Ya-Hui Chou[1,*], **Maria L. Spletter**[1,*], **Emre Yaksi**[2,*], **Jonathan C. S. Leong**[1], **Rachel I. Wilson**[2], and **Liqun Luo**[1]

Rachel I. Wilson: rachel_wilson@hms.harvard.edu; Liqun Luo: lluo@stanford.edu

[1] Howard Hughes Medical Institute, Department of Biology, Stanford University, Stanford, CA 94305

[2] Department of Neurobiology, Harvard Medical School, Boston, MA 02115

Abstract

Local interneurons play essential roles in information processing by neural circuits. Here we present a comprehensive genetic, anatomical, and electrophysiological analysis of local interneurons (LNs) in the *Drosophila* antennal lobe, the first olfactory processing center in the brain. We find that LNs are diverse in their neurotransmitter profiles, connectivity, and physiological properties. Analysis of >1500 individual LNs reveals major morphological classes characterized by coarsely stereotyped glomerular innervation patterns. Some of these morphological classes exhibit distinct physiological properties. However, the finer-scale connectivity of an individual LN varies considerably across brains and there is notable physiological variability within each morphological or genetic class. Finally, we show that LN innervation requires interaction with olfactory receptor neurons during development, and some individual variability also likely reflects LN-LN interactions. Our results reveal an unexpected degree of complexity and individual variation in an invertebrate neural circuit, a result that creates challenges for solving the *Drosophila* connectome.

Keywords

olfaction; glomerulus; variability; stereotypy; connectome

Neurons can be divided into two general categories: projection neurons whose axons connect discrete regions of neural tissue, and local interneurons whose processes are restricted to a single region. Local interneurons play an important role in neural computation. For example, horizontal and amacrine cells in the vertebrate retina are instrumental in transforming incoming signals from photoreceptors, such that information

Correspondence to: Rachel I. Wilson, `rachel_wilson@hms.harvard.edu`; Liqun Luo, `lluo@stanford.edu`.

*These authors contributed equally.

AUTHOR CONTRIBUTIONS: Y. C. and M.L.S. performed the anatomical and developmental experiments. E.Y. performed the physiological experiments. L.C.S.L. helped with statistical analysis. L.L. and R.I.W. supervised the project and wrote the paper.

regarding contrast, motion and color can be encoded by retinal ganglion cells and transmitted into the brain. Every vertebrate brain region contains a multitude of local interneurons, as defined by morphology, histological markers, and physiology, and likely distinct functions1. However, it is less clear whether the same kind of diversity exists in simpler organisms such as *Drosophila*. Systematic identification and characterization of local interneurons in the fly is a prerequisite to understanding information processing in neural circuits2.

The fly antennal lobe is an attractive model neural circuit because of its elegant anatomical and functional organization and its genetic tractability. All olfactory receptor neurons (ORNs) that express the same odorant receptor project their axons to the same antennal lobe glomerulus, and most antennal lobe projection neurons (PNs) send dendrites into a single glomerulus to receive direct input from one ORN class3. Genetic access is available to many classes of ORNs and PNs3. In contrast to these input and output neurons, local interneurons (LNs) in the fly antennal lobe are much less well characterized.

In the olfactory bulb, the vertebrate analog of the antennal lobe, there are ∼100 local interneurons for each projection neuron4, one of the highest local interneuron/projection neuron ratios in any mammalian brain region. Olfactory bulb interneurons are morphologically diverse and are hypothesized to play important roles in gain control, spike synchronization, and decorrelating the representations of similar odorants4-6. Studies of antennal lobe LNs in larger insects have described a variety of LN morphologies7-11. In comparison, the limited datasets available suggested that *Drosophila* antennal lobe LNs have relatively simple morphologies, with each LN innervating all glomeruli, although LNs which are not pan-glomerular have been described in more recent studies12-18. Understanding how ORN input is transformed into PN output by the antennal lobe requires a deeper understanding of antennal lobe LNs.

Here we take a systematic approach to identify and characterize LNs in the *Drosophila* antennal lobe. Using specific Gal4 lines in conjunction with the MARCM (Mosaic Analysis with Repressible Cell Marker) method19 and dye fills, we analyzed the morphology of >1,500 LNs at a single cell level. This analysis reveals a striking diversity of glomerular innervation patterns, which can be used to define distinct morphological classes of LNs. Major morphological LN classes have distinctive electrophysiological properties that help define their potential functions within the circuit. At a fine scale, our analysis also demonstrates that the innervation pattern of an individual LN varies across brains. Similarly, even within a morphologically- or genetically-defined class of LNs, we find considerable variability in physiological properties. This individual variation may in part reflect the role of cell-cell interactions during development. Our findings imply that LNs play unexpectedly diverse roles in olfactory processing in the fly antennal lobe. The wiring variability of LNs suggests that the wiring diagram differs considerably between individual fly brains, and that individual variations in behavior may in part reflect these kinds of fine-scale variations at the cellular level.

Results

Antennal lobe LNs and their neurotransmitter profiles

We used 10 Gal4 lines to genetically access antennal lobe LNs. The expression patterns of these lines span a range from hundreds of neurons near the antennal lobe to just a handful of LNs (Fig. 1). For simplicity, we refer to these Gal4 lines as Lines 1-10 (see Methods). In addition to LNs—which we define as neurons whose cell bodies are near the antennal lobe and whose processes are restricted to the antennal lobes—several lines also label ORNs, PNs and/or neurons near the antennal lobe that project to other areas of the brain (Supplementary Fig. 1 online).

LN cell bodies are located in two clusters: a large but continuous cluster lateral and dorsolateral to the antennal lobe (most LNs labeled by Lines 1, 3-9), and a separate cluster ventral to the antennal lobe (most LNs labeled by Line10) (Fig. 1, Supplementary Fig. 1 online). To determine the number and the potential overlap of LNs labeled by these Gal4 lines, we counted the number of nuclei labeled by UAS-nuclear marker driven from individual Gal4s, as well as from their combinations in the same fly (Supplementary Table 1 online). These data suggest that some lines label largely non-overlapping LN populations, whereas other lines overlap partly or completely.

Line5 appears to include all cells that are labeled by Lines 6-9. All ∼56 cells labeled by Line5 are LNs because 1) Line5 driven mCD8-GFP does not label any neurons that send processes out of the antennal lobe (Fig. 1), and 2) all 578 single cells from systematic MARCM analysis and biocytin fill (see below) from Line5 have their entire arborization within the antennal lobe. Based on the total number of LNs labeled by Lines 3, 4 and 5 in the same fly (Supplementary Table 1 online) and cell body positions from neuroblast clone analysis (Supplementary Fig. 1 online), we estimate that there are ∼100 LNs labeled by Lines 1 and 3-9, which are mostly ipsilaterally projecting LNs in the lateral cluster (see below). Line10 labels mostly bilaterally projecting LNs (see below) in the ventral cluster. Therefore, the lower bound for *Drosophila* LNs (labeled by our Gal4 lines) is ∼100 ipsilaterally projecting and ∼100 bilaterally projecting LNs for each antennal lobe.

Although LNs are traditionally considered to be inhibitory neurons that release GABA as their neurotransmitter, recent studies have suggested that some LNs can be excitatory14, 20 and cholinergic14, 17. We examined the neurotransmitter type of different Gal4 lines by co-staining with antibodies against GABA and Choline acetyltransferase. Antibody specificity was validated by loss of staining in MARCM clones homozygous mutant for *Glutamic acid decarboxylase 1* and *Choline acetyltransferase* (Supplementary Fig. 2a-h online). We found that the vast majority of LNs are GABAergic; however, there are a few cholinergic cells, and a larger minority that are neither GABAergic nor cholinergic (Supplementary Table 1 online; Supplementary Fig. 2i-l online). Staining for additional neurotransmitter types identifies a few dopaminergic and a large number of (mostly ventral) glutamatergic LNs (Supplementary Fig. 3 online). These results indicate that although the large majority of LNs are GABAergic, some LNs use different neurotransmitters or their combinations, emphasizing the potential diversity in the functional roles of different LNs.

Morphological diversity of LNs

The MARCM method can be used to label single neurons born at specific developmental times21, 22. We performed systematic MARCM labeling of LNs from these 10 Gal4 lines throughout development. Figure 2 shows representative images from 1,439 single cell LN clones. As is evident, LNs exhibit remarkable morphological diversity.

We identified 5 broad categories of ipsilaterally projecting LNs based on the extent of their arborization in the antennal lobe: the entire antennal lobe (pan-glomerular; Fig. 2a), all but a few glomeruli (Fig. 2b), a continuous region of the antennal lobe (Fig. 2c), discontinuous or patchy regions of the antennal lobe (Fig. 2d), 1-3 glomeruli (few-glomerular; Fig. 2e). Within each category, however, there is considerable diversity. For example, although many LNs arborize nearly the entire antennal lobe, they differ in the density of arborization and the thickness of their processes (Fig. 2a-b; Supplementary Fig. 4a-c online). For LNs that skip a few glomeruli or arborize in a continuous region, different individuals skip different glomeruli or arborize in different regions of the antennal lobe (Fig. 2b-c; Supplementary Fig. 5 online). Finally, bilaterally projecting LNs exhibit heterogeneous ipsilateral and contralateral arborization patterns (Fig. 2f).

Subcellular distribution of presynaptic terminals in LNs

Since all neurotransmitter release of LNs occurs within the antennal lobe, does each LN releases neurotransmitter throughout its arbor, or only in a restricted zone? To examine how presynaptic terminals are distributed within individual LNs, we performed a large subset of MARCM single cell labeling with an additional synaptotagmin-HA marker that labels presynaptic terminals23. In general, synaptotagmin-HA labels puncta throughout an LN's processes (red staining in Fig. 2, Supplementary Fig. 4 online). These data suggest that as a general rule, LNs broadcast transmitter release across their arborization without notable glomerular selectivity. However, in exception to this rule, some few-glomerular and bilateral LNs have a more selective synaptotagmin-HA distribution (Fig. 2e-f, Supplementary Fig. 4f online). These LNs therefore appear to deliver information to only a subset of glomeruli they innervate.

Statistical analysis of glomerular innervation patterns

Given the diversity of morphologies, we next analyzed these data systematically with the aim of identifying organizational principles of the LN network. An important feature of an LN is its glomerular innervation pattern, as this determines which olfactory channels the LN may receive information from and send information to. We therefore started by analyzing the glomerular innervation patterns of individual LNs.

We scored 1,532 individual LNs (1,439 from MARCM single cell clones; 93 from dye fills during whole cell patch clamp recording) for their innervation of 54 glomeruli in the antennal lobe (Fig. 3b). We employed hierarchical clustering to organize the 1,532 LNs according to their binary ipsilateral glomerular innervation patterns. This analysis revealed several distinct morphological classes (Fig. 3a). For example, neurons within subcluster C tend to avoid certain glomeruli innervated by trichoid ORN classes that sense pheromones24 (Fig. 3c). Neurons within subcluster D innervate the central antennal lobe and skip the

dorsal and ventral glomeruli; we call these dumbbell cells after their shape (Fig. 3d). Neurons within subcluster E exhibit patchy innervation (Fig. 3e).

Clustering all cells labeled by the same Gal4 (Supplementary Fig. 6 online) reveals that some Gal4 lines label a relatively uniform morphological population of cells (e.g. Lines 6-8), whereas others label a more heterogeneous group (e.g. Lines 1, 2, 3, and 5). This suggests that some Gal4 lines predominantly label LNs belonging to just a few functional classes, whereas others label a functionally heterogeneous population. We will examine this idea in more detail using electrophysiological recordings (see below).

Clustering all GABA+ vs. GABA- cells from our collection revealed that both subtypes include a diversity of morphological patterns (Supplementary Fig. 7 online). Because most LNs are GABAergic, we considered the hypothesis that LN innervation might be denser in glomeruli that receive more ORN input. We estimated the average lifetime activity of each ORN type based on a published dataset25 by averaging the responses of each ORN type across 110 odor stimuli. We found a significant positive correlation between LN innervation probability and mean odor-evoked ORN firing rate (Fig. 3f). This would be consistent with the idea that the density of inhibitory innervation is adapted to the average level of afferent input to each glomerulus26, assuming that these stimuli are representative of natural odors.

In addition to hierarchical clustering, we used principal component analysis (PCA) to identify emergent relationships in the glomerular innervation dataset without any arbitrary threshold of significance. The first and second principal components (PC1 and PC2; Fig. 3g and Supplementary Fig. 8 online) for the entire set of innervation patterns accounted for 40% and 10% of the variance in the data, respectively, but 13 additional principal components were needed to account for an additional 25%. The high number of dimensions necessary to account for variations indicates that innervation patterns are not well described as the linear combination of any small number of basic glomerular relationships. PC1 is essentially a proxy for the number of glomeruli innervated (correlation coefficient=0.9993). Thus, a defining feature of an LN's innervation pattern is the number of glomeruli it connects to. LNs were bimodally distributed on PC2, with a distinctive subcluster containing mainly dumbbell cells (Fig. 3d), confirming that the dumbbell cells constitute a distinctive morphological class.

Next, we considered the LNs that arborize bilaterally. We compared ipsilateral innervation patterns (Supplementary Fig. 9a online) with corresponding contralateral innervation patterns (Supplementary Fig. 9b online). We found that many bilateral LNs have rather symmetric glomerular innervation patterns and overall, ipsi- and contralateral patterns were significantly correlated (Pearson's correlation coefficient, r=0.46±0.05 (SEM), $p<0.01$, n=38) (Supplementary Fig. 9c online). In general, the exceptions were LNs with nearly pan-glomerular ipsilateral innervation.

Finally, based on clustering we identified a minimal number of LN classes with identifiable innervation patterns and further investigated birth timing and Gal4 expression for those cell types (Supplementary Fig. 5 online, Supplementary Table 2 online). We found that some (although not all) morphological types of LNs are labeled by only a few Gal4 lines and are

born in limited time windows. Together, these analyses indicate that LNs are composed of genetically distinct groups of cells defined by a combination of morphology, birth timing and Gal4 expression.

Diversity and stereotypy of physiological properties

Do LN genetic categories (Gal4 lines) and morphological categories (glomerular innervation patterns) have any correlation with physiological properties? To address this, we selected five Gal4 lines that label relatively small subsets of LNs (Lines 5-9) and made whole-cell patch-clamp recordings from GFP-labeled somata in each line. We recorded the responses of each cell to a panel of diverse odors (see Methods), and filled each cell with biocytin via the patch pipette for visualization after recording. We successfully filled and scored the innervation patterns of 93 LNs.

All these LNs fired spontaneous action potentials, and their spiking was always modulated by odors. LN odor responses were remarkably diverse and typically varied more across cells than across odors within a cell (Fig. 4a,b). Some LNs recorded in the same Gal4 line responded to odors in a similar manner (Fig. 4a). For example, the LNs we recorded in Line7 were relatively stereotyped in their functional properties, as were Line8 LNs. In other cases, a Gal4 line could label LNs having very different response profiles (Fig. 4b). Line5 and Line9 were particularly diverse in this respect.

In all these LNs, we measured spontaneous firing rate, mean odor response, and maximum odor response. To quantify the time course of the odor response, we also measured the percentage of spikes fired during the first 100 msec of the odor response. All four of these properties were significantly dependent on Gal4 lines (Fig. 4c). This implies that differences in Gal4 expression reflect physiological differences between LNs, in spite of the variability within each Gal4 line and the partial overlap in the cells that are labeled by these lines.

Physiological differences between morphological classes

Next, we asked whether LN physiological properties are correlated with their morphological class. Because the principal axis for morphological variation is the number of glomeruli each LN innervates (Fig. 3g), we began by asking whether any response properties were correlated with this axis. Unexpectedly, LNs that innervate many glomeruli have lower odor-evoked firing rates than LNs that innervate fewer glomeruli. The number of glomeruli innervated by an LN is significantly (although weakly) anti-correlated with the average strength of its odor responses (Pearson's $r=-0.2$, $p<0.05$).

This finding motivated us to examine the physiology of pan-glomerular LNs in particular, because these cells innervate the largest number of glomeruli. This class comprised 28% of the cells we recorded from. On average, pan-glomerular LNs had significantly higher spontaneous firing rates than other LNs (Fig. 5b). In the presence of an odor, spontaneous spiking in many pan-glomerular cells shut down completely, sometimes after a brief burst at odor onset, while others modestly increased their firing rate in the presence of odors (Fig. 5a). Overall, odor-evoked changes in firing rate were significantly weaker in pan-glomerular cells that in other LNs (Fig. 5b).

A second major class of LNs that we recorded from were LNs that selectively avoid glomerulus VA1d and frequently also avoid DL3 (Fig. 3c). These glomeruli are innervated by trichoid ORNs thought to be selective for pheromones24. This innervation pattern (with slight variations) accounts for ∼15% of all LNs in our data set from Lines 1-7, notably those labeled by Line6 (Fig. 3a; see below), and 10% of cells we filled in electrophysiological recordings. These cells differed from other LNs in having especially transient bursts of excitation at odor onset (Fig. 5c). Overall, this morphological class fired a higher percentage of their spikes in the first 100 msec of the response, as compared to other LNs (Fig. 5d). Thus, these LNs could create a transient pulse of GABAergic inhibition at odor onset. If so, then some pheromone glomeruli would evidently be selectively excluded from this transient pulse of inhibition.

Line6 LNs: coarse stereotypy and fine variability

Does the diversity we observe in LN morphology and physiology arise from variability of the same LNs across different individual animals, or from many diverse LN types each with stereotypic patterns in all individuals? The first alternative is implied by our finding of 847 distinct innervation patterns in 1,489 ipsilateral-projecting LNs (Fig. 3a), far exceeding the number of estimated total ipsilateral-projecting LNs (∼100) within an individual antennal lobe. LN arborization patterns therefore cannot be completely stereotyped across animals.

We sought to address this question by dense sampling of a Gal4 line (Line6) that labels a small population (7 LNs per antennal lobe, Supplementary Table 1 online). Of 131 labeled single cells for Line6, we observed 76 distinct glomerular innervation patterns (Fig. 6a). Since there are many more innervation patterns than the number of cells per animal, individual Line6 labeled LNs cannot be identical across animals.

Electrophysiological recordings showed that Line6 LNs also have diverse functional properties (Fig. 6b-e and 5c). Some cells (Fig. 6b,c) showed a transient burst at the onset of almost every odor, followed by inhibition. Other cells (Fig. 6d,e) exhibited sustained excitation, off-excitation, and more odor-specific tuning. Thus, neither the morphology nor the physiology of Line6 LNs is highly stereotyped.

Despite the clear evidence that individual LNs labeled by Line6 are not rigidly stereotyped, the properties of these LNs are far from randomly distributed. For example, the odor response properties of Line6 cells are significantly less varied across cells than the odor response properties of all LNs. Mean and maximum odor-evoked firing rates were less variable within the Line6 population (n=16) than across the LN population as a whole (n=92, $p<5\times10^{-5}$, F-tests). In addition, spontaneous firing rates were also less variable within the Line6 population than across all LNs ($p<5\times10^{-6}$, F-test).

The glomerular innervation patterns of Line6 LNs are also far from random. Each Line6 LN innervates 51.1 glomeruli (n=131, SEM=0.22) on average. If the innervation pattern were completely random, then every glomerulus would have a 94.4% probability of being innervated. Assuming a binomial probability distribution, the number of samples innervating a glomerulus should vary by the standard error, ±2%. The actual distribution clearly deviates from this prediction (Fig. 6f). Most glomeruli are almost always innervated, whereas a

subset of glomeruli is often missed. Among this latter group of glomeruli, VA1d is most often omitted. Indeed, most of the biocytin-filled LNs that selectively avoided VA1d (Fig. 5d) were Line6 LNs (7 of 9).

Since our binary scores for innervation patterns are only a coarse measure of a LN's morphology, we additionally measured the innervation density of Line6 LNs for selected glomeruli that are either always innervated or often missed. We found that DM1 (always innervated) has a significantly higher innervation density compared to VA1d or DA1 (occasionally innervated), whereas randomly selected pan-glomerular LNs exhibit similar innervation density of DM1, VA1d and DA1. Innervation density of Line6 neurons in DA1 and VA1d glomeruli is significantly reduced compared with that of pan-glomerular LNs (Fig. 6g). These data strengthen the distinction of these two groups of glomeruli with regard to Line6 LN innervation. One group is always innervated, while the other group has highly reduced innervation if not completely avoided.

In summary, analysis of Line6 indicated a principle likely applicable to most other morphologically and genetically-defined classes of LNs. LNs exhibit marked variability within a class, and some of this variability must represent variations in the same cells across different brains. Yet the properties of these LNs are clearly not drawn randomly from the entire distribution of LN properties. This picture is consistent with the idea that the coarse properties of these cells are genetically pre-programmed, whereas their finer-scale properties may also reflect factors such as developmental plasticity and sensory experience.

Patchy LNs: a potential mechanism for variability

The variability of glomerular innervation patterns is exemplified in a small subset of LNs from Lines 1, 3, and 5 that exhibit a distinctive pattern of patchy innervation (Fig. 2d, 3e). Strikingly, comparison of the glomerular innervation patterns of 161 patchy cells (Fig. 7a) indicates that none of these single cells innervate identical sets of glomeruli. Given that these patchy cells represent only a small fraction of cells labeled by LN Gal4s and a small fraction of the ~100 ipsilaterally projecting LNs, it is clear that the innervation patterns of patchy LNs are highly variable across different animals.

The patchy nature of these cells suggested that these innervation patterns might be established through cell-cell interactions among LNs. To examine the relationships between innervation patterns of different LNs in the same animal, we designed a genetic method to visualize a pair of sister patchy cells with two different colors in the same animal (Fig. 7b). Although the efficiency of this method was extremely low, yielding only 5 pairs of patchy cells after thousands of dissected brains, it is evident that processes of sister patchy cells avoid each other to carve out their innervation domains, sometimes by splitting a single glomerulus (outlined in Fig. 7c-e, Supplementary Fig. 10 online). By contrast, differentially labeled sister cells of other LN types inter-mix at much finer scales (Fig. 7f-h). We confirmed the qualitative difference by quantifying the degree of overlap between the signals of the two cells after the signals had been systematically dilated to varying degrees (see Methods). Non-patchy cells exhibited a great deal of overlap with just a small amount of dilation, while patchy cells exhibited similar degrees of overlap only after they had been dilated much more (Fig. 7i). These observations suggest that sister patchy LNs may tile the

antennal lobe the way ganglion cells tile the vertebrate retina27 and sensory neurons tile the *Drosophila* body wall28. We also estimated that each patchy LN occupies 13.1±1.6% (mean ±SD, *n*=8) of the antennal lobe volume, implying that eight patchy LNs could tile an entire antennal lobe. These findings suggest that LN-LN interactions play a role in establishing patchy LN morphologies.

Development and maintenance of LN innervation patterns

Finally, we tested the contributions of ORNs to the glomerular arborization pattern of LNs. During the construction of the antennal lobe circuit, PN dendrites initiate pattern formation by targeting dendrites to positions similar to where they are found in the adult antennal lobe before the arrival of pioneering axons. ORN axon invasion into the antennal lobe and subsequent ORN axon-PN dendrite recognition results in the formation of distinguishable glomeruli29, 30. The development of LNs has not previously been described.

We first tested whether LN arborization during pupal development requires ORN axons. We made use of the fact that Hedgehog signaling is required for antennal disc proliferation, and clonal loss of Smoothened, a component essential for Hedgehog signaling, results in occasional loss of maxillary palps while leaving the antennae intact30. Under this condition, ORN axons from the antennae would innervate glomeruli that are normal targets of antennal ORN axons, but glomeruli that are normal targets of maxillary palp ORNs are devoid of ORN input30. By introducing Line5 Gal4 driven mCD8-GFP into this genetic background and screening for flies with bilateral loss of maxillary palps (∼1 in 250; Fig. 8a), we found that LN processes are not present in the glomeruli that are normal targets of maxillary palp ORNs. LN processes still innervate the nearby glomeruli that are targets of antennal ORNs (Fig. 8b, bottom panels, compared to Fig. 8b, top panels; Fig. 8d). By contrast, PN dendritic processes are mostly still present in glomeruli devoid of ORN axons (Fig. 8c, d). This experiment suggests that glomerular innervation of LNs requires the presence of ORN axons.

To test whether the ORN axons are required for the maintenance of LN processes, we bilaterally removed the maxillary palps in adults, well after antennal lobe wiring is completed. We examined the processes of Line6 LNs (which are a subset of Line5 LNs) at least 10 days after removal of the maxillary palps to allow complete degeneration of ORN axons. We found that LN processes still innervate maxillary palp glomeruli (Fig. 8e). The volume of one of the two glomeruli quantified is significantly reduced (Fig. 8f, top panel), likely because ORN axons contribute to the glomerular volume31. However, the total length of LN processes and the total number of presynaptic terminals as marked by synaptotagmin-HA puncta are unaffected by the adult removal of ORNs (Fig. 8f, middle and bottom panels). We also compared variability of glomerular innervation patterns of Line6 LNs between wild-type flies and those with ORNs removed. We found no significant differences in the number of glomeruli innervated or unique innervation patterns (Supplementary Fig. 11 online), suggesting that variability of Line6 LNs is not dependent on the presence of ORN axons in adult. Taken together, these experiments indicate that ORN axons are essential for LN innervation during development, but are not required for the maintenance of their glomerular innervation in adulthood.

Discussion

Knowledge of local interneuron properties is essential to understand how a neural circuit processes information. Here we present a systematic single-cell analysis of >1500 antennal lobe LNs in *Drosophila*. The scale of our analysis is an order of magnitude greater than the most comprehensive analysis of insect LNs published to date8. Our genetic strategy also avoided sampling biases involved with dye filling, which favors large cells with easy access. Despite the caveat that our sampling of LNs is not entirely even (see Methods), our study revealed a striking diversity of antennal lobe LNs beyond that described previously in any insect. LNs are diverse in their neurotransmitter types, glomerular innervation patterns, fine dendritic structures, densities and distribution of presynaptic terminals, and odor response properties. Furthermore, our analysis of glomerular innervation patterns and odor responses revealed coarse stereotypy but also a surprising degree of fine-scale variability in genetically-defined subclasses of LNs. Below we discuss the implications of these findings for the development and function of the antennal lobe circuit, and for the complexity of the *Drosophila* brain as a model for neural circuit analysis.

How is the morphological diversity of LNs established?

The final glomerular innervation patterns of LNs likely result from some combination of: 1) genetic specification, 2) cell-cell interactions during development, and 3) neuronal activity and plasticity. Our study suggests that these mechanisms are used differentially in specifying different aspects of LN diversification. We also cannot rule out additional contributions of sex, age and rearing conditions (see Methods).

We envision that the distinctions between major LN categories are specified largely by genetic mechanisms similar to those used to specify other types of central neurons, such as antennal lobe PNs. These include neuroblast lineage, birth timing, and specific gene expression. For example, most bilateral projecting LNs have cell bodies located ventral to the antennal lobe, are labeled by Line10, and derive from a distinct neuroblast (Supplementary Fig. 1 online). All patchy LNs are born during a well-defined time window in the mid-larval stage (Supplementary Fig. 5 online, Supplementary Table 2 online) and are derived exclusively from Lines 1, 3, and 5. Dumbbell cells derive exclusively from Lines 1, 2, and 9, and are also born during a defined larval stage (Supplementary Fig. 5 online, Supplementary Table 2 online). At a finer level, even though Line6 LNs exhibit a large number of glomerular innervation patterns, these patterns are biased against certain pheromonal glomeruli. Furthermore, the density of arborization and presynaptic terminals within glomeruli that are always innervated is higher than those that are only occasionally innervated by Line6. One can imagine that mechanisms that translate lineage and birth timing to wiring specificity of PNs and other glomerular targeting mechanisms32 can also be used to specify glomerular innervation specificity of certain types of LNs.

Compared to ORNs and PNs, however, LN glomerular innervation patterns are much more variable and less deterministic. The most striking example is patchy LNs: the 161 single cells we examined exhibited 161 distinct glomerular innervation patterns. Our two-cell clone analysis suggests a developmental mechanism for achieving this diversity. We found that processes of sister patchy cells tend to avoid each other even when they innervate common

glomeruli. Our quantitative analysis is consistent with the idea that these complex dendrites tile the three-dimensional volume of the antennal lobe. These data suggest that homophilic repulsion might play a role in establishing final innervation patterns of some LN morphological types. From a functional perspective, it seems likely that the specific glomerular innervation patterns of individual patchy LNs are unimportant as long as a group of similar types of patchy LNs cover the entire antennal lobe.

Functional Implications

Local interneuron classes defined by morphology and molecular markers are thought to have distinct functions1. The *Drosophila* antennal lobe represents an unusual opportunity to assess *in vivo* the functional correlates of LN classes. Overall, we found that LNs varied widely in their odor-evoked firing rates and their temporal dynamics. The selective modulation of LNs with particular dynamics could be a way to modulate the temporal pattern of PN activity.

On a coarse level, some physiological diversity correlated with differences in morphology or genetic markers. For example, pan-glomerular LNs had unusually high rates of spontaneous activity, suggesting that they may be particularly important in broadcasting tonic inhibition throughout the antennal lobe. Tonic inhibition is thought to regulate the sensitivity of odor detection in the mammalian olfactory bulb33, 34. Pan-glomerular LNs were either inhibited by odors or were only weakly excited. Because they are mainly GABAergic, inhibition of pan-glomerular LNs would tend to disinhibit the entire antennal lobe in response to odors.

To take another example, LNs that avoid certain pheromone-selective glomeruli fired unusually transient bursts at odor onset. These LNs may have a special role in inhibiting the initial 100 msec of PN odor responses, when PN firing rates peak35. Some pheromone glomeruli are evidently excluded from this inhibition. This may reflect the fact that pheromones elicit weaker peak firing rates as compared to other odors24, and may help explain why weak pheromone responses are strongly amplified in postsynaptic PNs36.

Although we found a coarse correlation between some functional properties and morphological or genetic classifications, we also found that each LN class we examined in finer detail contained substantial diversity. For example, both pan-glomerular and pheromone-avoiding LNs had varied odor responses. Similarly, Line6 LNs were also heterogeneous, especially considering that there are only ∼7 such cells. Thus, we are unlikely to be able to accurately predict every aspect of an LN's physiology based solely on its morphology or a few molecular markers. Interestingly, interneurons of the mammalian cortex are also remarkably varied, prompting the remark that “inhibitory cells seem to be so diverse as perhaps to endanger the notion of cell types in the central nervous system”37. Here we have shown that interneuron diversity in the *Drosophila* brain rivals that of the mammalian brain, and we have begun to establish developmental principles underlying this diversity.

Complexity of the *Drosophila* Brain

It is widely believed that, compared to vertebrates38, invertebrate nervous systems are much more stereotyped across different members of the same species, with individually identifiable neurons and stereotyped connection patterns. Indeed, previous analysis of projection patterns of individual antennal lobe PNs provided a striking example in support of this notion39, 40. Thus, the degree of variability of glomerular innervation patterns of individual LNs came as a surprise. Such variability should translate into variability in the functional connectivity of LNs, ORNs and PNs.

While the glomerular organization of the antennal lobe provides a convenient and unequivocal demonstration of variability in the *Drosophila* "connectome", it remains to be determined whether variable connectivity is a general feature of the fly brain. Interestingly, even the axons of antennal lobe PNs, which exhibit strikingly stereotyped terminal arborization patterns in the lateral horn, display less stereotypy in the mushroom body23, 39, 40. Indeed, a recent physiology study suggests non-stereotypic connections between PN axons and their postsynaptic targets in the mushroom body41. It is possible that, upon detailed examination, such lack of stereotypy is the norm rather than an exception even in the relatively simple insect brain.

We and others42 believe that a wiring diagram is a necessary (although certainly not sufficient) prerequisite for understanding the function of neural circuits. However, our results imply that the complete reconstruction of the wiring diagram of a single *Drosophila* brain will not yield a general wiring diagram for all *Drosophila* brains. At the same time, our findings identify a fundamental similarity between insect and vertebrate brains in the variability of their connectomes. Although it may prove more challenging than previously assumed to map the connectivity of the fly brain, solving the *Drosophila* connectome may turn out to be more relevant to understanding our own brain.

Methods

Gal4 lines

Line1 (HB4-93) and Line6 (HB8-145) were identified from an anatomical screen of an unpublished Gal4 library from Ulrike Heberlein. Line2 (NP6277) and Line5 (NP3056) were ordered from the NP Gal4 library[44] based on our various unpublished screens. Line7 (LCCH3) is an unpublished line from Julie Simpson. Other lines have been described before for their expression in LNs or in other brain neurons: Line3=H24[45]; Line4=GH298[46]; Line8=Nan-Gal4[47]; Line9=krasavietz-Gal4[48]; Line10=OK10721.

Single cell collections

Our 1,532 single cells from 10 Gal4 lines were collected over the course of two years so experimental conditions vary. Most MARCM analysis used 0-14 day old female flies except Lines 2, 3 and 10 where a subset of experiments were performed with male flies, and Line 9 used exclusively males. A subset of Line6 single cell clones were collected after antennae and/or maxillary palps were removed, so these flies as well as their untreated controls were dissected between 10-20 days after eclosion. All electrophysiology experiments were

performed using 2-3 day old females. Flies were reared at 25°C for MARCM experiments and at room temperature for physiology experiments.

It is important to note that the relative frequency of single cells in our collection does not necessarily reflect the fraction of these cells in a given animal because of our sampling bias with regard to Gal4 lines and heatshock windows—the number of MARCM-labeled single cells is not proportional to the number of LNs in a given Gal4 line, and not all developmental windows are equally sampled.

MARCM, Immunostaining, Image Processing

MARCM analysis was performed according to established protocols19. Briefly, MARCM ready stocks were crossed, eggs collected for various lengths of time (ranging from 2-24 hours), and samples heat-shocked at time points of interest during embryonic, larval and early pupal development. Heatshocks at middle and late pupal stages rarely induced LN clones in our early experiments and thus were not employed further. Heat-shock time windows for all cells are listed in Supplementary Table 2. Adult brains were dissected, fixed and stained as described before22. After staining, brains were mounted in SlowFade Gold (Molecular Probes) and imaged on a Zeiss Meta-510 confocal. Images were processed using LSM software (Zeiss) and Image J (http://rsbweb.nih.gov/ij/). Further measurements including glomerular volume, dendrite length and synaptotagmin-HA density (Fig. 6, Fig. 8) were made in Imaris (Bitplane) and statistical analysis performed in Excel and Graphpad Prism 5.0 software. To determine the volume of the antennal lobe occupied by individual patchy cells, LSM software was used to trace the outline of the antennal lobe (marked by N-cadherin) or patchy cell processes (labeled by GFP or CD2) in each confocal section collected at 1 mm intervals. The volume was determined as the sum of areas from each 1 mm section. Cell counts were performed manually or with the aid of Imaris.

Primary antibodies used include: rat anti-mCD8a (1:100, Invitrogen), chicken anti-GFP (1:1000; Aves Labs), rabbit anti-GFP (1:1000, Molecular Probes), mouse anti-nc82 (1:30, Developmental Studies Hybridoma Bank [DSHB]), mouse anti-rCD2 (1:100, OX34, Serotec), rat anti-N-cadherin (1:40, DN-EX #8, DSHB), mouse anti-HA (1:100, 12CA5, gift of Dr. K. Wehner), rabbit anti-HA (1:1000, Abcam), rabbit anti-βgal (1:1000, CAPPEL/MB Biomedicals), chicken anti-βgal (1:1000, Abcam), mouse anti-Cha (1:100, ChAT4B1, DSHB), rabbit anti-GABA (1:200, Sigma), rabbit anti-DVGLUT(1:500; gift of Dr. A. DiAntonio). Secondary antibodies from Molecular Probes (MP) or Jackson ImmunoResearch Laboratories (JIRL) and used at 1:500 include: Zenon mouse Cy5 (MP), goat anti-mouse Cy3 (JIRL), goat anti-rat Alexa488 (MP), goat anti-rat Cy5 (JIRL), goat anti-rat Cy3 (JIRL), goat anti-rabbit Alexa488 (MP), goat anti-rabbit Cy5 (JIRL), donkey anti-chicken FITC (JIRL), donkey anti-chicken Cy3 (1:300, JIRL).

Physiology

Whole-cell patch-clamp recordings from LN somata were performed as previously described13. External saline contained (in mM): 103 NaCl, 3 KCl, 5 N-tris(hydroxymethyl) methyl-2-aminoethane-sulfonic acid, 8 trehalose, 10 glucose, 26 $NaHCO_3$, 1 NaH_2PO_4, 1.5 $CaCl_2$, and 4 $MgCl_2$ (osmolarity adjusted to 270-275 mOsm). The saline was bubbled with

95% O2/5% CO2 and reached a pH of 7.3. The internal patch-pipette solution contained (in mM): 140 potassium aspartate, 10 HEPES, 4 MgATP, 0.5 Na3GTP, 1 EGTA, 1 KCl, and 13 biocytin hydrazide. The pH of the internal solution was adjusted to 7.3 and the osmolarity was adjusted to ∼ 265 mOsm. LN somata were targeted by means of the GFP signal under epifluorescent illumination in an Olympus BX51WI microscope with a 40X water-immersion objective. Spontaneous firing rates were measured in cell-attached mode prior to whole-cell break-in. After break-in, a small amount of hyperpolarizing current was injected constantly to compensate for the seal conductance and thereby to return the cell to its native spontaneous firing rate[49]. Recordings were acquired with an A-M Systems Model 2400 amplifier in current clamp mode (10MΩ headstage), low-pass filtered at 2 kHz, and digitized at 10 kHz. One neuron was recorded per brain and the morphology of each cell was visualized post hoc with biocytin-streptavidin and nc82 histochemistry as described previously35 using a Zeiss LSM 510 META confocal microscope.

The total number of LNs recorded in each Gal4 line (and the number whose biocytin fills were successfully reconstructed) was: Line5 55 recorded (51 reconstructed), Line6 18 (17), Line7 21 (11), Line8 8 (5), Line9 11 (8). In some of these cells, we did not complete the full set of physiological measurements, which is why the number experiments cited in connection with some statistical tests is smaller than the numbers listed here. We emphasize that this distribution is not necessarily representative of the actual underlying distribution of these LNs. For example, we deliberately over-sampled Line5 in an attempt to try to hit some of the unusual morphological types labeled by this line (including patchy, dumbbell, and “few-glomerular” LNs). Despite these attempts, we were not able to record from any of these particular morphological classes of LNs, either for technical reasons (e.g., their somata may be unusually small, or they may express low levels of GFP) or potentially due to a low abundance of these morphological classes. Thus, a systematic comparison of all morphological and physiological categories was not possible. The physiological diversity we describe is therefore only a lower bound on the diversity of the LN population.

Odors (Sigma) were delivered with a custom olfactometer, as described previously35. All odors were diluted 1:100 v/v in paraffin oil, and the odor vial headspace was diluted 10-fold in air before reaching the fly. We chose a panel of 10 odors to maximize the chemical diversity of our stimuli, to maximize overlap with odors used in other studies of the same ORNs, and to activate a wide variety of ORN types to varying degrees[50]. Spike times were extracted and converted to PSTHs by binning them in 50-msec counting windows that overlapped by 25 msec. Each odor was presented 6 times at intervals of 40–60 sec and those trials were then averaged to generate a PSTH for that odor/cell combination. Where the odor response of a cell is expressed as a single time-averaged firing rate, these rates were measured over a 1-sec period beginning at odor onset, and are expressed as a change in firing rate relative to the spontaneous firing rate of that cell. Analyses were performed in IgorPro and in MATLAB.

Statistical Analysis of Glomerular Innervation Patterns

Scoring data in clustering analyses were collected manually by examining individual planes of 1 μM z-stacks. 54 antennal glomeruli, as depicted in Fig. 3b, were identified in the nc82

or N-cadherin channel. A glomerulus was considered innervated if any green-colored LN process entered the nc82/N-cadherin dense region of a glomerulus.

Hierarchical clustering of innervation data was performed using freely available Cluster (http://bonsai.ims.u-tokyo.ac.jp/~mdehoon/software/cluster/software.htm) or R (http://www.r-project.org/) software. Data were clustered using complete linkage and a Euclidean distance measure in either program. Results were visualized as dendrograms and heatmaps using JavaTreeView (http://jtreeview.sourceforge.net/) or native R graphics facilities. The coherence of clusters was assayed in R using bootstrap analysis available through the pvclust package with n≥5000 at p-value>95% and at p-value>90%. Hierarchical clustering was verified by comparison to iterative k-means based clustering. k was determined for each iteration by plotting the within groups sum of squares or by using the GAP statistic. Clusters identified by hierarchical clustering that correlate with those revealed by iterative k-means based clustering were judged significant.

Innervation data were also imported into Matlab R2007a (Mathworks), where principal component analysis (PCA) was performed using customized software. Data were centered by subtracting off column means but were not rescaled.

Theoretical probabilities for LN6 innervation were calculated based on the assumption that all glomeruli have an equal chance of being innervated. Thus, for a given set of n innervation patterns, the chance a given glomerulus is innervated = (the total number of innervated glomeruli in the dataset/54)/n. Assuming that the collection of innervation probabilities is binomially distributed, the variation in observations can be calculated as the standard error = √[p*(1-p)/n], where p = probability of innervation and n = number of samples. These theoretical probabilities are presented in Fig. 6f as the average % innervation by glomerulus ± standard error as the upper and lower bounds.

We use the following intuition to quantify the overlap between patchy and non-patchy sister cells. For non-patchy sister cells colored red and green, a given volume of the antennal lobe of small size should contain both red and green signal, while for patchy sister cells, the same volume of antennal lobe could conceivably contain just red or just green signal. Only if the volume of interest were much larger should the strength of the overall red and green signals within the volume of interest become more comparable. To test this idea, cell bodies and brain regions outside the antennal lobe were first excluded from the analysis. An intensity threshold was then applied to sister cell image stacks to isolate the innervation patterns from background with all pixels below the 97.5th percentile set to 0. Such thresholded images were then dilated using cube shaped kernels of varying size. For image vectors $\vec{r}$ and $\vec{g}$, an index of overlap *OI* was computed as follows:

$$OI(\vec{r},\vec{g})=\frac{\sum_{x,y,z}\vec{r}\,(x,y,z)\cdot\vec{g}\,(x,y,z)}{\|\vec{r}\|\cdot\|\vec{g}\|}=\cos(\theta)$$

using the Euclidean norm and where θ is the angle between r and $\bar{g}$. Finally, we plotted the overlap index as a function of dilation kernel size.

Perturbation Experiments

To eliminate both maxillary palps in early development, *smo*^{3} mutant clones were induced by eyFLP in flies expressing Line5 or GH146-Gal4 driven mCD8GFP. Adults missing both MPs but retaining both antennae were dissected and their brains were analyzed for LN or PN innervation in glomeruli targeted by MP ORNs.

To remove ORN input in adults, MARCM ready Line6 flies were heat-shocked between 24-72h after egg laying to generate single cell LN clones. Antennae, maxillary palps or both were severed and removed between 0-2 days after eclosion using a #5 forceps. Flies were aged between 10-20 days before dissection and immunohistochemistry. Confocal images were loaded into Imaris where individual glomeruli were traced to obtain volumetric measurements. LN projection length within individual glomeruli as well as Syt-HA puncta were also quantified using Imaris.

Data Access

All the raw data used for clustering, including the confocal stacks of all LNs in Supplementary Tables 2 and 3, are accessible at http://flybrain.stanford.edu.

Supplementary Material

Refer to Web version on PubMed Central for supplementary material.

Acknowledgments

We thank Ulrike Heberlein and Lisa Marin respectively for providing and screening unpublished Gal4 lines which lead to identification of Line1 and Line6; Julie Simpson for providing unpublished LCCH3 (Line7) Gal4; the Bloomington Stock Center, Kyoto Stock Center, NIG (GETDB), and Developmental Studies Hybridoma Bank for other reagents. We are grateful for the help of Jess Brooks in data collection and the Stanford Department of Statistics Consulting Service for technical help with statistical analyses. We thank Tom Clandinin, Greg Jefferis, and members of the Luo and Wilson labs for helpful comments on the manuscript. This work was supported by NIH grants to L.L. (R01-DC005982) and R.I.W. (R01-DC008174), a Pew Scholar Award, a McKnight Scholar Award, a Sloan Foundation Research Fellowship, and Beckman Young Investigator Award (to R.I.W). M.L.S. is an NRSA predoctoral fellow. E.Y. is supported by a Human Frontiers Science Program Long Term Fellowship. J.C.S.L. is supported by the Medical Scientist Training Program at Stanford University. L.L. is an investigator of the Howard Hughes Medical Institute.

References

1. Markram H, et al. Interneurons of the neocortical inhibitory system. Nat Rev Neurosci. 2004; 5:793–807. [PubMed: 15378039]
2. Olsen SR, Wilson RI. Cracking neural circuits in a tiny brain: new approaches for understanding the neural circuitry of Drosophila. Trends Neurosci. 2008; 31:512–520. [PubMed: 18775572]
3. Vosshall LB, Stocker RF. Molecular architecture of smell and taste in Drosophila. Annu Rev Neurosci. 2007; 30:505–533. [PubMed: 17506643]
4. Shepherd, GM.; Chen, WR.; Greer, CA. Olfactory Bulb. In: Shepherd, GM., editor. The synaptic organization of the brain. Oxford University Press; Oxford: 2004.
5. Lledo PM, Merkle FT, Alvarez-Buylla A. Origin and function of olfactory bulb interneuron diversity. Trends Neurosci. 2008; 31:392–400. [PubMed: 18603310]

6. Wachowiak M, Shipley MT. Coding and synaptic processing of sensory information in the glomerular layer of the olfactory bulb. Semin Cell Dev Biol. 2006; 17:411–423. [PubMed: 16765614]
7. Christensen TA, Waldrop BR, Harrow ID, Hildebrand JG. Local interneurons and information processing in the olfactory glomeruli of the moth Manduca sexta. J Comp Physiol [A]. 1993; 173:385–399.
8. Seki Y, Kanzaki R. Comprehensive morphological identification and GABA immunocytochemistry of antennal lobe local interneurons in Bombyx mori. J Comp Neurol. 2008; 506:93–107. [PubMed: 17990273]
9. MacLeod K, Laurent G. Distinct mechanisms for synchronization and temporal patterning of odor-encoding neural assemblies. Science. 1996; 274:976–979. [PubMed: 8875938]
10. Fonta C, Sun XJ, Masson C. Morphology and spatial distribution of bee antennal lobe interneurons responsive to odours. Chem Senses. 1993; 18:101–119.
11. Ernst KD, Boeckh J. A neuroanatomical study on the organization of the central antennal pathways in insects. III. Neuroanatomical characterization of physiologically defined response types of deutocerebral neurons in Periplaneta americana. Cell Tissue Res. 1983; 229:1–22. [PubMed: 6831538]
12. Stocker RF, Lienhard MC, Borst A, Fischbach KF. Neuronal architecture of the antennal lobe in Drosophila melanogaster. Cell Tissue Res. 1990; 262:9–34. [PubMed: 2124174]
13. Wilson RI, Laurent G. Role of GABAergic inhibition in shaping odor-evoked spatiotemporal patterns in the Drosophila antennal lobe. J Neurosci. 2005; 25:9069–9079. [PubMed: 16207866]
14. Shang Y, Claridge-Chang A, Sjulson L, Pypaert M, Miesenbock G. Excitatory local circuits and their implications for olfactory processing in the fly antennal lobe. Cell. 2007; 128:601–612. [PubMed: 17289577]
15. Ng M, et al. Transmission of olfactory information between three populations of neurons in the antennal lobe of the fly. Neuron. 2002; 36:463–474. [PubMed: 12408848]
16. Lai SL, Awasaki T, Ito K, Lee T. Clonal analysis of Drosophila antennal lobe neurons: diverse neuronal architectures in the lateral neuroblast lineage. Development. 2008; 135:2883–2893. [PubMed: 18653555]
17. Das A, et al. Drosophila olfactory local interneurons and projection neurons derive from a common neuroblast lineage specified by the empty spiracles gene. Neural Develop. 2008; 3:33.
18. Okada R, Awasaki T, Ito K. Gamma-aminobuyric acid (GABA)-mediated neural connections in the Drosophila antennal lobe. J Comp Neurol. 2009; 514:74–91. [PubMed: 19260068]
19. Lee T, Luo L. Mosaic analysis with a repressible cell marker for studies of gene function in neuronal morphogenesis. Neuron. 1999; 22:451–461. [PubMed: 10197526]
20. Olsen SR, Bhandawat V, Wilson RI. Excitatory interactions between olfactory processing channels in the Drosophila antennal lobe. Neuron. 2007; 54:89–103. [PubMed: 17408580]
21. Lee T, Lee A, Luo L. Development of the Drosophila mushroom bodies: sequential generation of three distinct types of neurons from a neuroblast. Development. 1999; 126:4065–4076. [PubMed: 10457015]
22. Jefferis GSXE, Marin EC, Stocker RF, Luo L. Target neuron prespecification in the olfactory map of Drosophila. Nature. 2001; 414:204–208. [PubMed: 11719930]
23. Jefferis GS, et al. Comprehensive maps of Drosophila higher olfactory centers: spatially segregated fruit and pheromone representation. Cell. 2007; 128:1187–1203. [PubMed: 17382886]
24. van der Goes van Naters W, Carlson JR. Receptors and neurons for fly odors in Drosophila. Curr Biol. 2007; 17:606–612. [PubMed: 17363256]
25. Hallem EA, Carlson JR. Coding of odors by a receptor repertoire. Cell. 2006; 125:143–160. [PubMed: 16615896]
26. Sachse S, et al. Activity-dependent plasticity in an olfactory circuit. Neuron. 2007; 56:838–850. [PubMed: 18054860]
27. Wassle H, Peichl L, Boycott BB. Dendritic territories of cat retinal ganglion cells. Nature. 1981; 292:344–345. [PubMed: 7254331]

28. Grueber WB, Jan LY, Jan YN. Tiling of the Drosophila epidermis by multidendritic sensory neurons. Development. 2002; 129:2867–2878. [PubMed: 12050135]
29. Jefferis GS, et al. Developmental origin of wiring specificity in the olfactory system of Drosophila. Development. 2004; 131:117–130. [PubMed: 14645123]
30. Sweeney LB, et al. Temporal target restriction of olfactory receptor neurons by Semaphorin-1a/PlexinA-mediated axon-axon interactions. Neuron. 2007; 53:185–200. [PubMed: 17224402]
31. Berdnik D, Chihara T, Couto A, Luo L. Wiring stability of the adult Drosophila olfactory circuit after lesion. J Neurosci. 2006; 26:3367–3376. [PubMed: 16571743]
32. Luo L, Flanagan JG. Development of continuous and discrete neural maps. Neuron. 2007; 56:284–300. [PubMed: 17964246]
33. Pirez N, Wachowiak M. In vivo modulation of sensory input to the olfactory bulb by tonic and activity-dependent presynaptic inhibition of receptor neurons. J Neurosci. 2008; 28:6360–6371. [PubMed: 18562606]
34. Shao Z, Puche AC, Kiyokage E, Szabo G, Shipley MT. Two GABAergic intraglomerular circuits differentially regulate tonic and phasic presynaptic inhibition of olfactory nerve terminals. J Neurophysiol. 2009; 101:1988–2001. [PubMed: 19225171]
35. Bhandawat V, Olsen SR, Gouwens NW, Schlief ML, Wilson RI. Sensory processing in the Drosophila antennal lobe increases reliability and separability of ensemble odor representations. Nat Neurosci. 2007; 10:1474–1482. [PubMed: 17922008]
36. Schlief ML, Wilson RI. Olfactory processing and behavior downstream from highly selective receptor neurons. Nat Neurosci. 2007; 10:623–630. [PubMed: 17417635]
37. Miles R. Perspectives: neurobiology. Diversity in inhibition. Science. 2000; 287:244–246. [PubMed: 10660424]
38. Lu J, Tapia JC, White OL, Lichtman JW. The interscutularis muscle connectome. PLoS Biol. 2009; 7:e32. [PubMed: 19209956]
39. Marin EC, Jefferis GSXE, Komiyama T, Zhu H, Luo L. Representation of the glomerular olfactory map in the Drosophila brain. Cell. 2002; 109:243–255. [PubMed: 12007410]
40. Wong AM, Wang JW, Axel R. Spatial representation of the glomerular map in the *Drosophila* protocerebrum. Cell. 2002; 109:229–241. [PubMed: 12007409]
41. Murthy M, Fiete I, Laurent G. Testing odor response stereotypy in the Drosophila mushroom body. Neuron. 2008; 59:1009–1023. [PubMed: 18817738]
42. Lichtman JW, Sanes JR. Ome sweet ome: what can the genome tell us about the connectome? Curr Opin Neurobiol. 2008; 18:346–353. [PubMed: 18801435]
43. Laissue PP, et al. Three-Dimensional Reconstruction of the Antennal Lobe in Drosophila melanogaster. J Comp Neuro. 1999; 405:543–552.
44. Hayashi S, et al. GETDB, a database compiling expression patterns and molecular locations of a collection of Gal4 enhancer traps. Genesis. 2002; 34:58–61. [PubMed: 12324948]
45. Martin JR, Ernst R, Heisenberg M. Mushroom bodies suppress locomotor activity in Drosophila melanogaster. Learn Mem. 1998; 5:179–191. [PubMed: 10454382]
46. Stocker RF, Heimbeck G, Gendre N, de Belle JS. Neuroblast ablation in Drosophila P[GAL4] lines reveals origins of olfactory interneurons. J Neurobiol. 1997; 32:443–456. [PubMed: 9110257]
47. Kim J, et al. A TRPV family ion channel required for hearing in Drosophila. Nature. 2003; 424:81–84. [PubMed: 12819662]
48. Dubnau J, et al. The staufen/pumilio pathway is involved in Drosophila long-term memory. Curr Biol. 2003; 13:286–296. [PubMed: 12593794]
49. Gouwens NW, Wilson RI. Signal propagation in Drosophila central neurons. J Neurosci. 2009; 29:6239–6249. [PubMed: 19439602]
50. Hallem EA, Ho MG, Carlson JR. The molecular basis of odor coding in the Drosophila antenna. Cell. 2004; 117:965–979. [PubMed: 15210116]

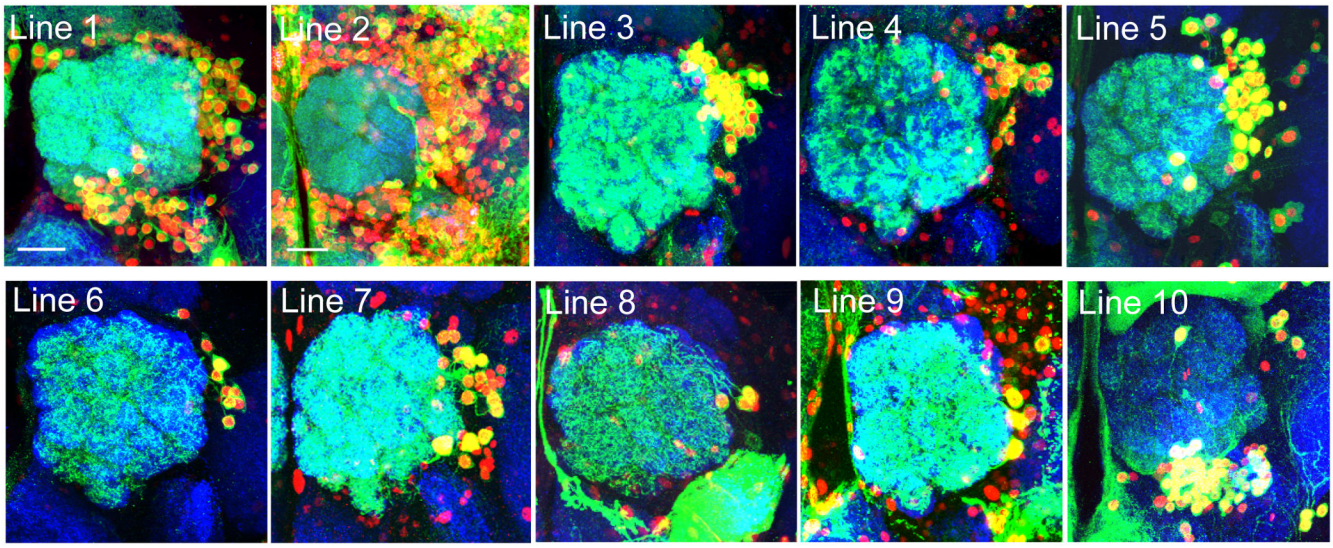

Figure 1. Antennal lobe LNs

Expression patterns of 10 Gal4 lines used in this study. Green, Gal4 driven mCD8-GFP; Red, Gal4 driven nuclear LacZ or nuclear RFP; Blue, neuropil staining by nc82. Scale bars, 20 μm.

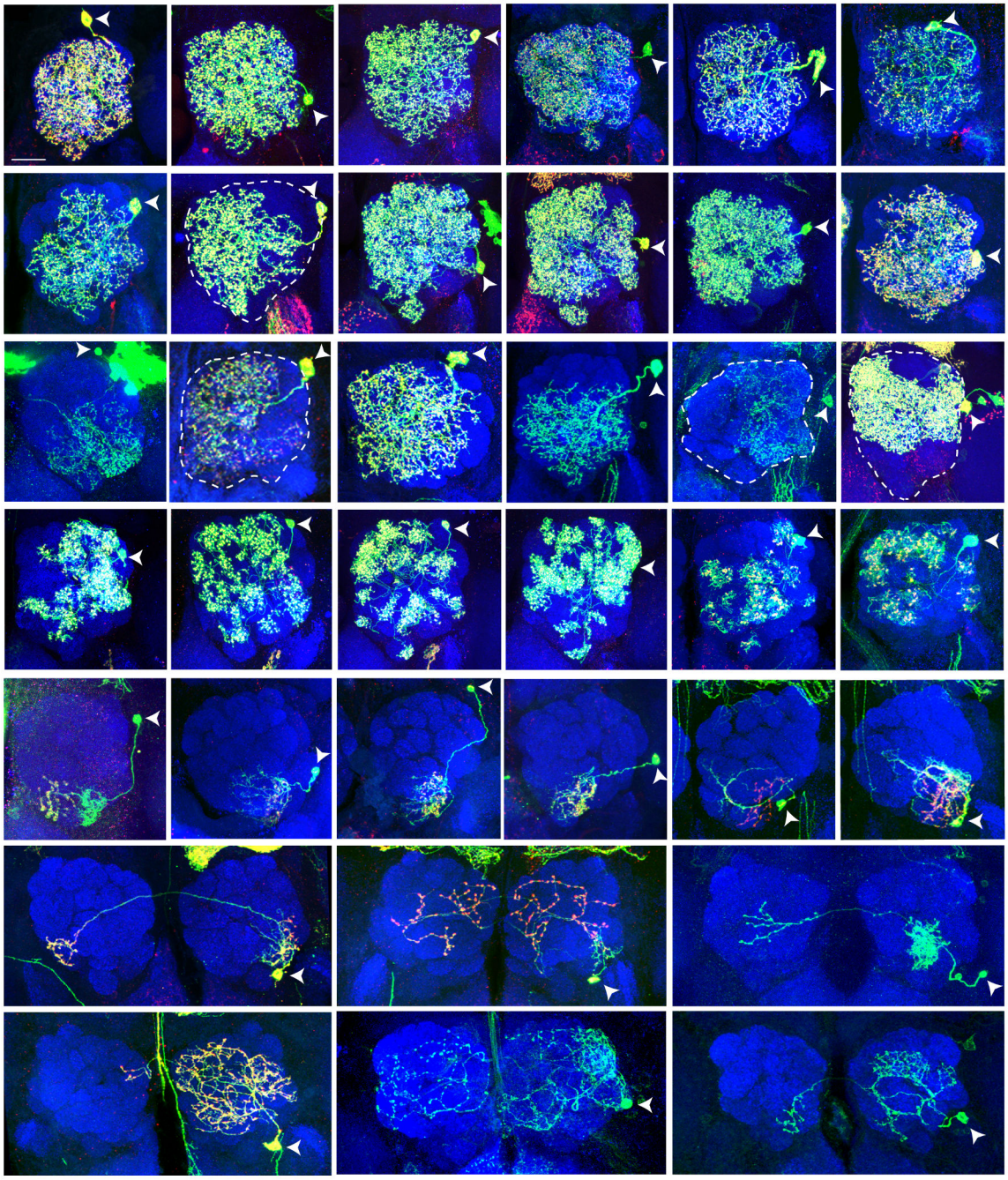

Figure 2. Diversity of LN morphology

(**a-e**) Representative arborization patterns of single cell MARCM clones of ipsilateral projecting LNs. Each row represents examples from categories that innervate: (**a**) all glomeruli, (**b**) all but a few glomeruli, (**c**) regional, (**d**) patchy, (**e**) a few glomeruli. (**f**) Representative arborization patterns of bilateral projecting LNs. Green, mCD8-GFP that labels LN processes; red, synaptotagmin-HA, a marker for presynaptic terminals; blue, nc82 or N-cadherin staining that highlight glomerular structures. Images in **c** (left, forth and fifth from left) and **f** (third, fifth and sixth from left) are not

stained for Syt-HA. Arrowheads indicate cell bodies. Dashed lines mark the outline of the antennal lobe. Scale bar, 20 μm. Information about corresponding Gal4 lines in this and subsequent figures can be found in Supplementary Table 4.

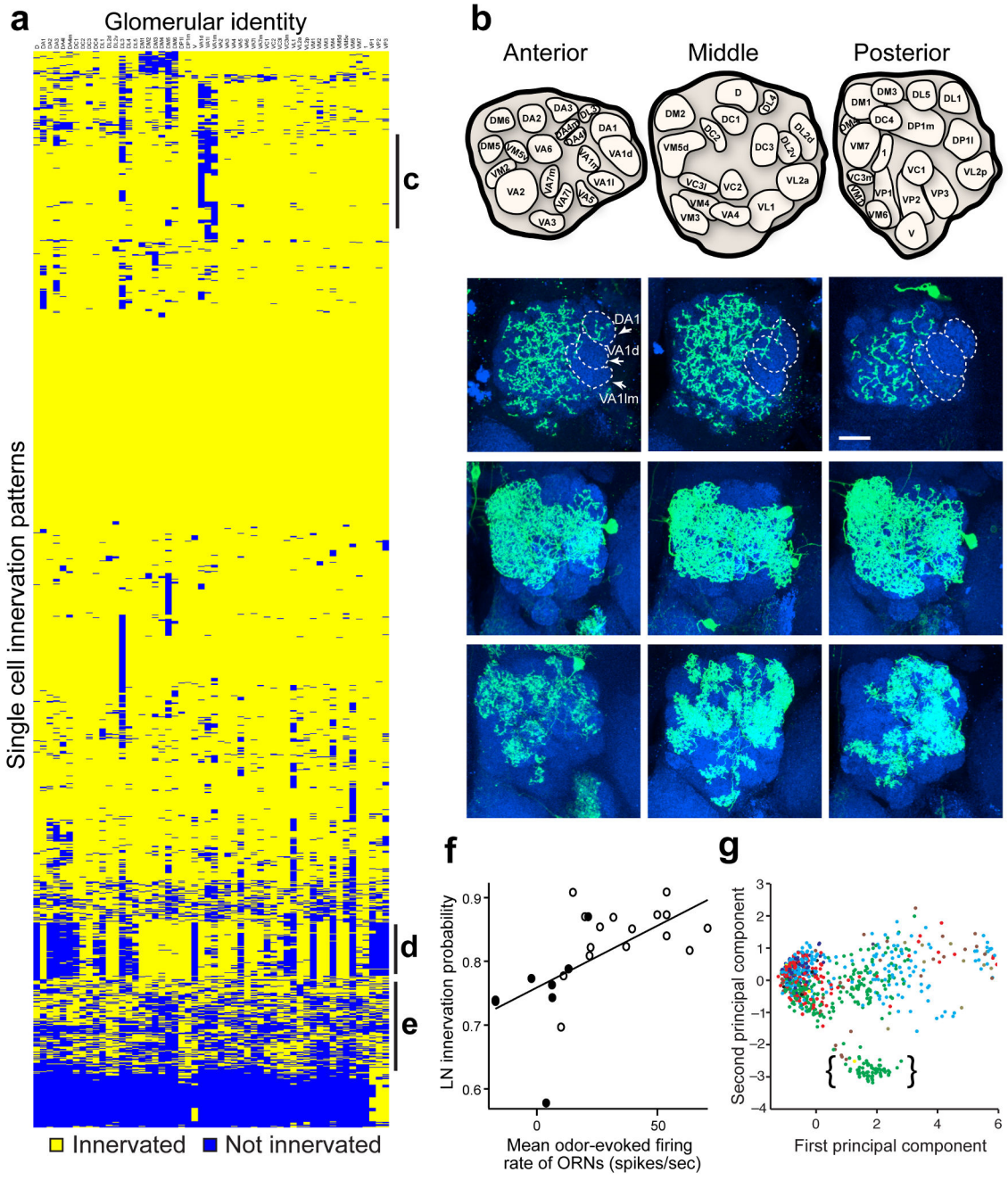

Figure 3. Statistical analysis of glomerular innervation patterns

(**a**) Binary glomerular innervation patterns of 1532 singly labeled LNs organized by hierarchical clustering. Rows represent innervation patterns of individual cells; columns represent 54 glomeruli. 1489 are ipsilateral projecting LNs. Of the 43 bilateral projecting LNs, only the ipsilateral patterns are included in the clustering analysis. Yellow, glomeruli innervated; blue, glomeruli not innervated.

(**b**) Antennal lobe model. The 54 glomeruli we scored for this study are outlined in three sections of the antennal lobe from anterior to posterior. This model is modified after a number of sources3, 43 and derived from tracing nc82 stained brains.
(**c-e**) Three representative images from three selective regions of the LN cluster diagram indicated on the right side of Fig. 3a. mCD8-GFP staining in green, nc82 or N-cadherin staining in blue. Dashed lines in (C) mark pheromonal glomeruli, DA1, VA1d and VA1l/m. Scale bar, 20μM.
(**f**) The LN innervation probability of a glomerulus is positively correlated with the mean odor-evoked firing rate of the ORNs presynaptic to that glomerulus (r=0.63, p<0.005, n=23 glomeruli). ORN data from ref25. Firing rates averaged across 110 odors. Filled symbols represent trichoid glomeruli.
(**g**) Principal component analysis of LN glomerular innervation patterns. In the second dimension, the dumbbell subclass of LNs (bracket) distinctly separates from all other cell types. LNs labeled by different Gal4 lines are marked with different colors. See Supplementary Fig. 8 for color code of Gal4 lines and histograms of cell distributions in PC1 and PC2.

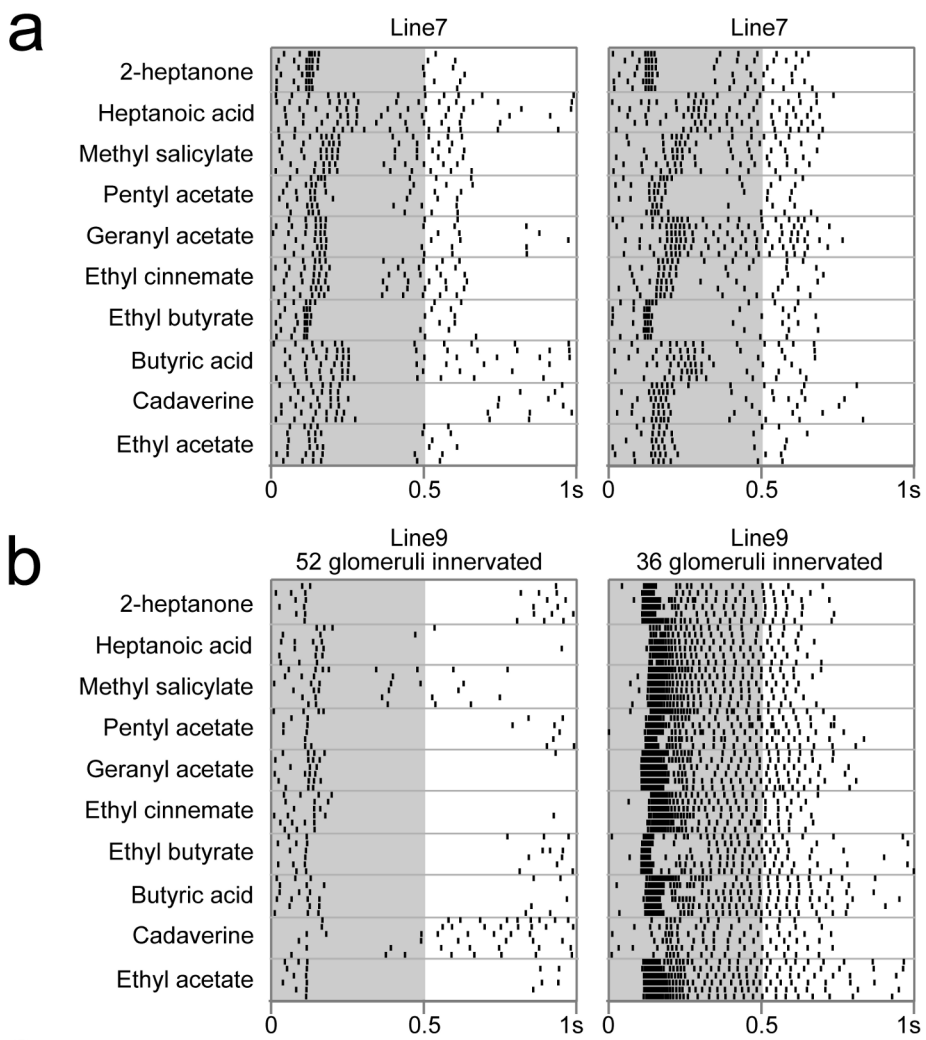

	Spontaneous firing rate (spikes per sec)	Maximum odor response (spikes per sec)	Mean odor response (spikes per sec)	Percentage of spikes in 1st 100ms of response
Line5	4.0 ± 0.4	15.7 ± 1.7	8.7 ± 1.4	14 ± 1
Line6	4.5 ± 0.7	7.0 ± 1.0	2.5 ± 0.6	21 ± 2
Line7	16.8 ± 1.7	1.5 ± 1.2	-3.1 ± 1.2	23 ± 2
Line8	5.2 ± 0.6	2.7 ± 1.1	-0.3 ± 0.7	43 ± 4
Line9	7.8 ± 2.1	18.1 ± 5.5	7.7 ± 3.5	17 ± 3

Figure 4. Functional stereotypy and diversity among genetic classes

(**a**) Rasters show the similar spiking responses of two Line7 LNs. These LNs are typical of Line7 in having high spontaneous firing rates, weak odor-evoked excitation, and strong odor-evoked inhibition. The nominal odor stimulus period is denoted by the gray box; there is a delay of about 100msec before odor reaches the fly.

(**b**) Dissimilar responses of two Line9 LNs. The first of these innervated almost all glomeruli (52 of 54) and was mainly inhibited by all odors, whereas the second innervated a smaller subset of glomeruli and was excited by all odors. Overall, Line9 LNs were diverse.

(**c**) Functional properties of Lines5-9 (mean±SEM). All these properties were significantly dependent on the Gal4 line of the recorded LN (one-way ANOVA, $p<0.0001$). For each property, *post hoc* Tukey tests yielded significant differences ($p<0.05$) between some but not all of the 10 pair-wise comparisons between Gal4 lines. Odor-evoked firing rates are expressed as a change from the spontaneous firing rate.

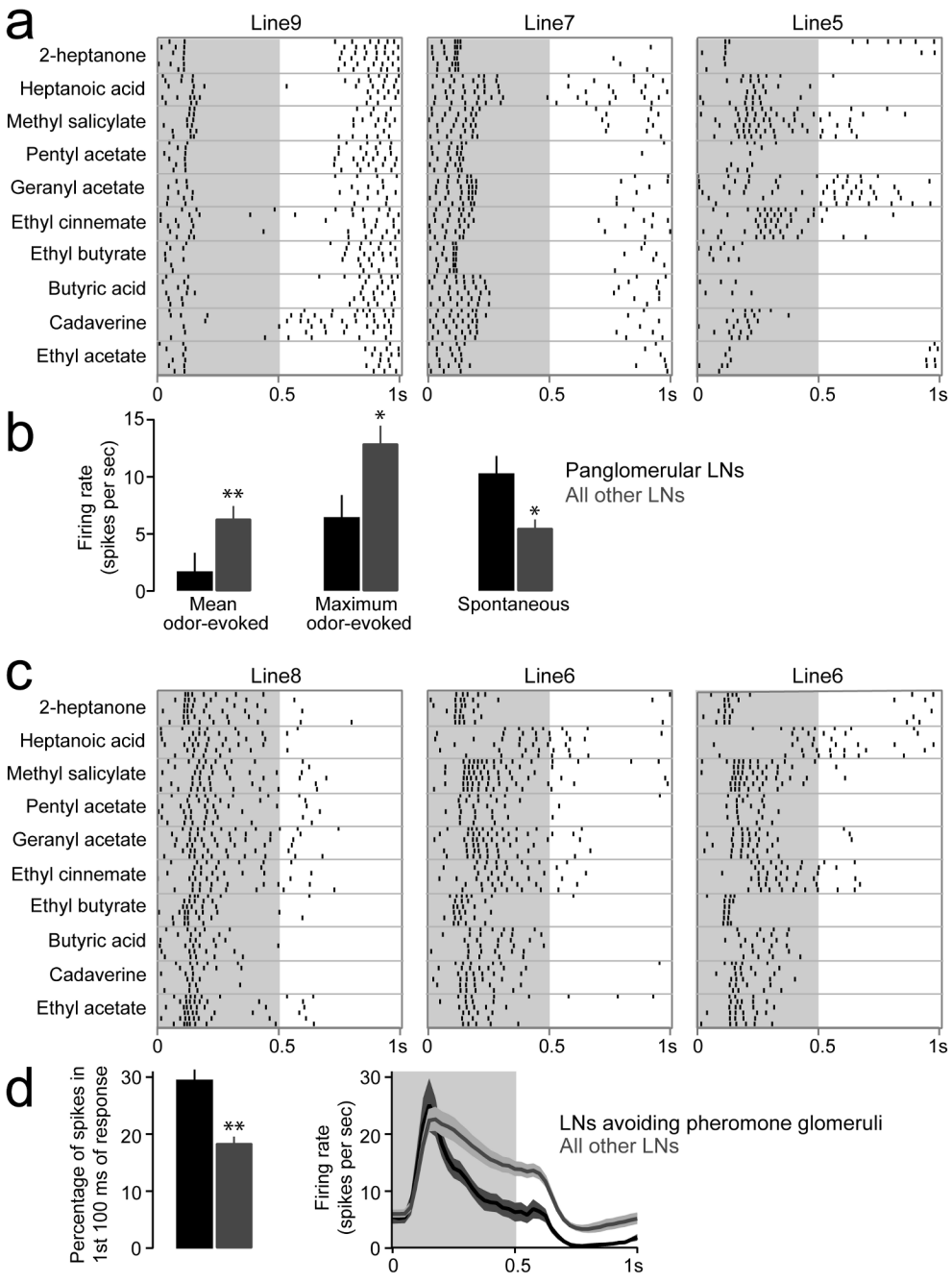

Figure 5. Functional differences between morphological classes

(**a**) Odor responses of three pan-glomerular LNs.

(**b**) Pan-glomerular LNs (*n*=26) have significantly higher spontaneous activity ($p<0.01$) and weaker mean and maximum odor responses ($p<0.05$, t-tests) as compared to all other LNs that were successfully reconstructed (*n*=67).

(**c**) Odor responses of three LNs that avoid glomerulus VA1d ± DL3 but innervate all other glomeruli (“pheromone-avoiding”).

(**d**) Left: pheromone-avoiding LNs (n=9) fire a significantly higher percentage of their spikes during the first 100ms of the odor response as compared to all other LNs (n=84) (p<0.01, t-test; spikes counted during the period 100-200msec after nominal odor onset, divided by total spikes during the 1-sec period shown in rasters). Right: odor response time course is more transient for these LNs than for other LNs (mean peri-stimulus time histogram, ±SEM across cells).

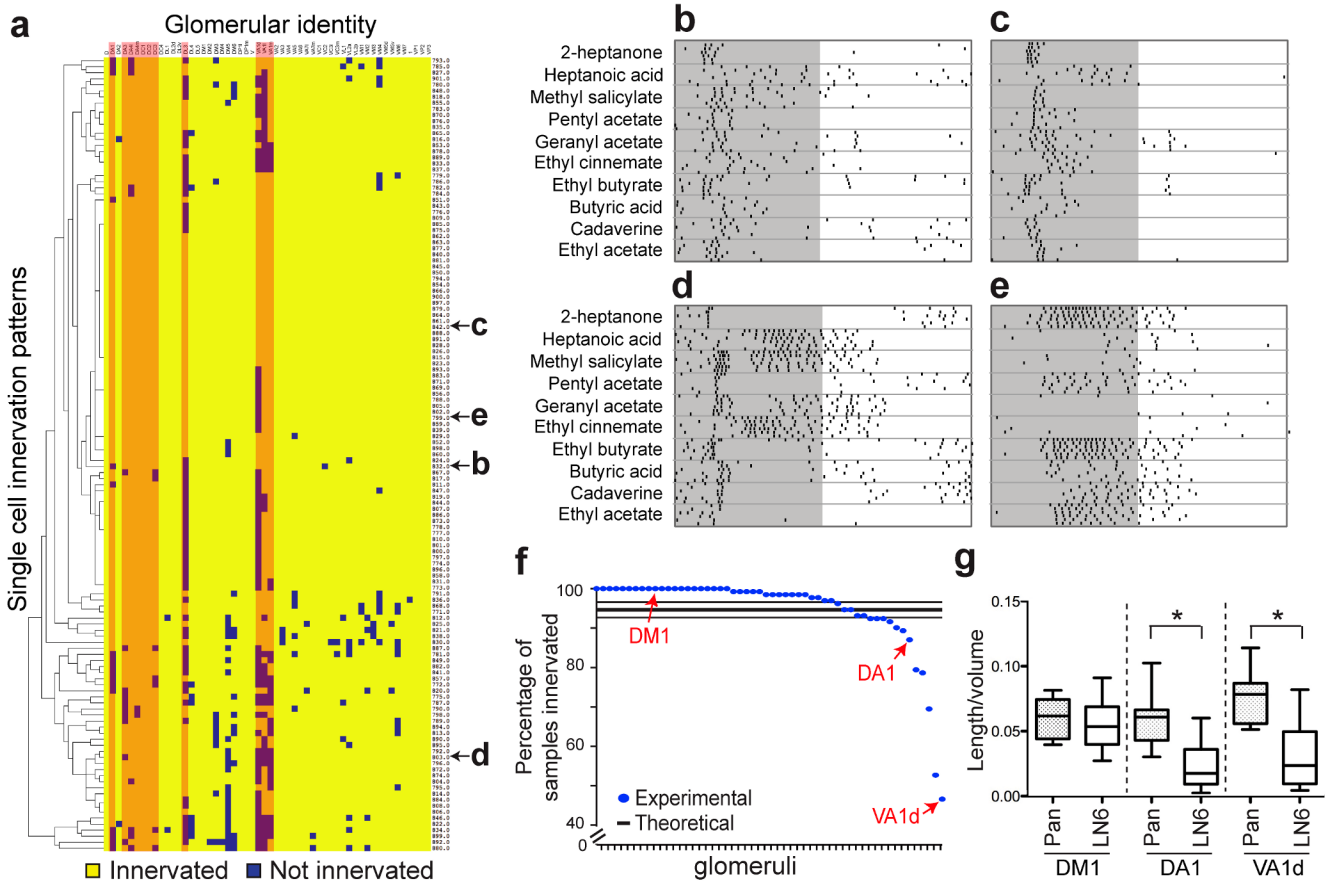

Figure 6. Variability and stereotypy of Line6 LNs

(**a**) Hierarchical clustering of innervation patterns as in Fig. 3a but only for Line6 LNs (*n*=131). Cells in (**b-e**) are indicated. Glomeruli innervated by trichoid ORNs (pheromonal glomeruli) are highlighted in orange. K-means clustering verified that Line6 binary innervation patterns form a single cluster. Some cells were from animals in which antennae, maxillary palps or both had been removed for 10 days prior to fixation (Fig. 8e-f), but these treatments did not affect the number or the variability of glomerular innervation (Supplementary Fig. 11).

(**b-e**) Odor response of four Line6 LNs. Shaded regions of plots denote odor stimulus period (500 ms).

(**f**) Comparison of experimental and theoretical frequency of innervation (center black line) if glomeruli were randomly innervated. The envelope of ±2% is the standard error assuming a binomial distribution of innervation frequencies. The experimental frequency (blue dots) reveals that many glomeruli are almost always innervated, significantly above the theoretical distribution; other glomeruli are innervated significantly less frequently than the theoretical distribution. The glomerular identities to the right of DA1 are DM5, VA1m, VA1l, DL3 and VA1d; all except DM5 are pheromonal glomeruli.

(**g**) Quantification of innervation density of DM1, DA1 and VA1d, from randomly chosen 10 LNs of each class that innervate all three glomeruli. Innervation density=total dendritic length in glomerulus/glomerulus volume. Innervation of DA1 and VA1d by Line 6 LNs is

significantly reduced compared to control LNs (pan-glomerular randomly selected from Lines 1, 3, 5), Tukey test, $p<0.05$.

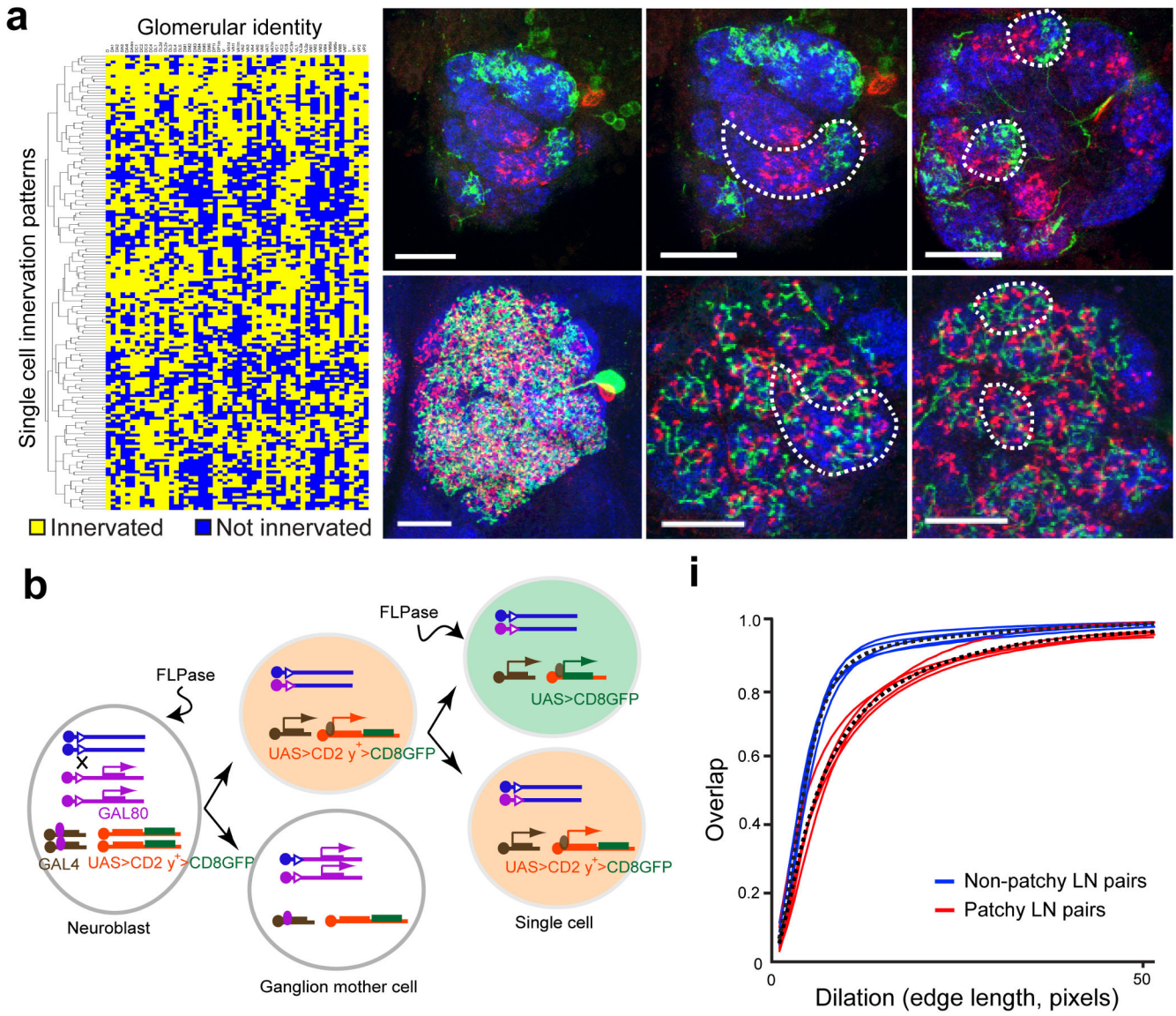

Figure 7. Variability of patchy LNs

(**a**) Clustering of 161 patchy cell innervation patterns as in Fig. 3a. No two cells have identical innervation patterns.

(**b**) Schematic of MARCM-FLPout that allows two sister cells to be labeled by different colors. In this genetic method, *UAS-FRT-CD2-FRT-mCD8GFP*40 serves as a reporter of Gal4. After FLP-mediated mitotic recombination causes the loss of Gal80 in the ganglion mother cell (GMC), CD2 should be expressed in both daughter cells derived from this GMC. However, if an additional FLPout event occurs in one of the two daughter cells, this cell will express mCD8-GFP instead of CD2.

(**c-h**) Examples of two sister patchy cells (**c-e**) and two sister control cells (**f-h**) labeled by MARCM-FLPout shown with N-cadherin (blue), GFP (green) and CD2 (red) staining. (**c, f**) Projection of the entire antennal lobe. (**d, e, g, h**) High magnification of 5 μm projections from anterior (**d, g**) and middle (**e, h**) antennal lobe sections showing non-overlapping

processes from 2 sister cells. Dashed lines mark the boundary of glomeruli VA1l/m (**d**), DL1 and DC2 (**e**). Scale bars, 20 μm.

(**i**) Sister cell overlap index as a function of edge length of the dilation kernel (see Methods). Dashed lines indicate the mean for patchy sister cells (right-shifted) and non-patchy sister cells (left-shifted). Colored lines indicate individual pairs of sister cells. A quantitative distinction between patchy and non-patchy classes was verified by K-means clustering into two clusters.

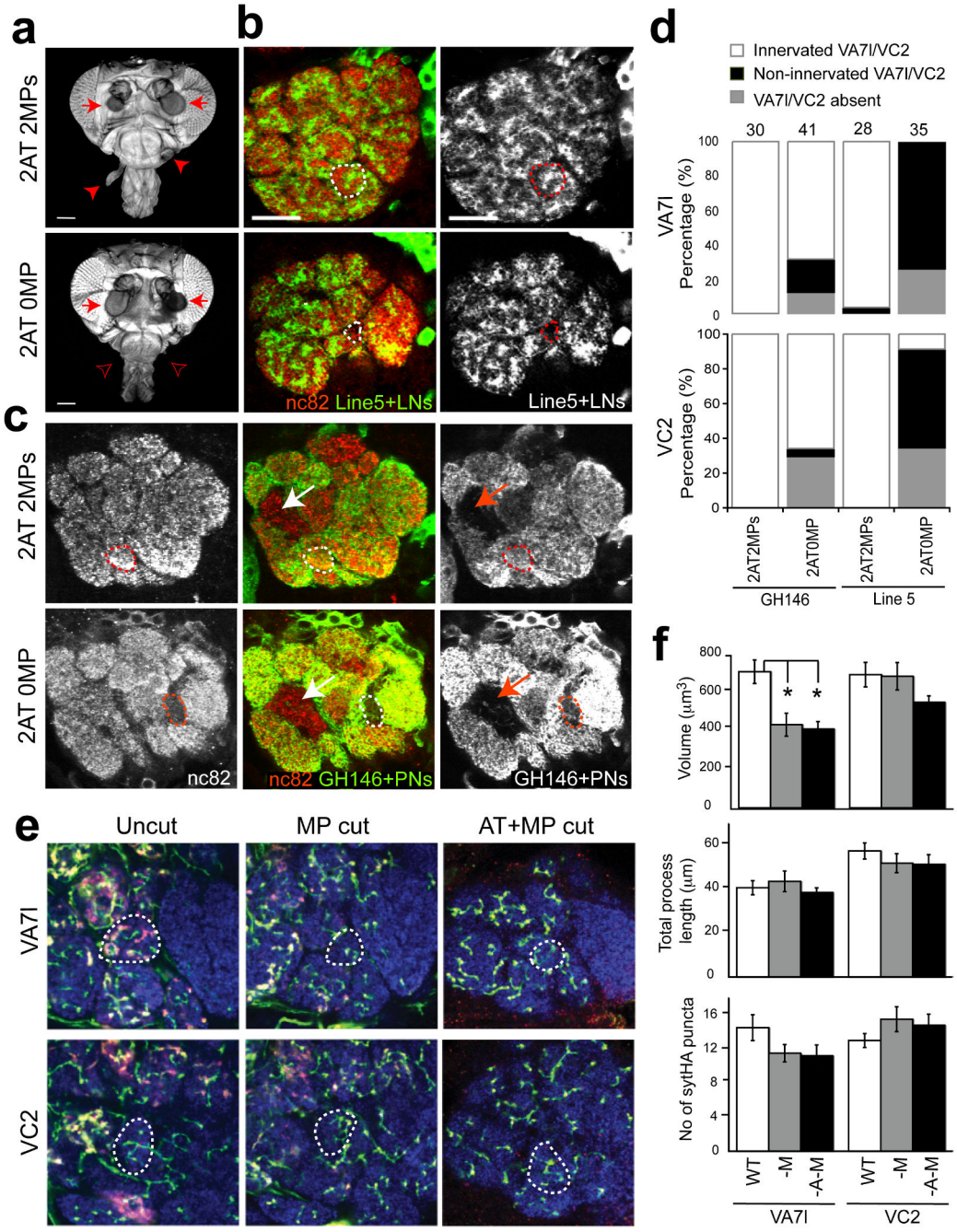

Figure 8. Development but not maintenance of LN arborization depends on ORNs

(**a**) (Top) A normal adult fly head with 2 antennae (AT, arrows) and 2 maxillary palps (MPs, arrowheads). (Bottom) Occasionally, eyFLP-induced *smo* clones eliminate both MPs (open arrowheads). Scale bars, 100μm.

(**b-c**) Brains from normal (top) and 0 MP (bottom) flies carrying *Line5-Gal4* (**b**) or *GH146-Gal4* (**c**) were labeled by nc82 and Gal4 driven mCD8GFP as indicated. The MP ORN target VA7l glomerulus (dotted circle) is not innervated by Line5 processes in 0MP flies, but

is still innervated by PN processes. Arrows designate glomeruli that are innervated by GH146-negative PNs. Scale bars, 20 μm.

(**d**) Quantification of glomerular innervation by Line5-Gal4 LN and GH146-Gal4 PN processes in the presence or absence of ORN innervation of MP target glomeruli VA7l (top) and VC2 (bottom).

(**e**) Representative single sections of Line6 LN single cell clones after adult removal of MPs, or MPs and ATs. Control samples (uncut) show clear Line6 LN innervation of VA7l (top) and VC2 (bottom). After adult removal of MPs or both MPs and AT, Line6 LNs still innervate VA7l and VC2. Blue, nc82; green, mCD8-GFP; red, Syt-HA.

(**f**) Quantification of glomerular volume, LN process length and the number of Syt-HA puncta in control (WT), MP cut (-M) or MP and AT cut (-A-M) brains. The VA7l volume is significant decreased when ORN processes are removed, but neither process length nor the number of Syt-HA puncta in VA7l and VC2 is significantly reduced. Error bars represent SEM.